laminar flow hood. Bilateral ovariectomy was performed under anesthesia by dorsolateral laparotomy. Human ovarian tissue was transplanted in the back skin, kidney capsule, and ovarian bursa in the same host animal. Two pieces of ovarian tissue were placed in each site. After transplantation, the ovarian bursa was closed by suturing with 9-0 nylon. No antibiotics were used. Ten weeks following transplantation, intraperitoneal injection of human menopausal gonadotropin (HMG, Humegon; Organon, Oss, The Netherlands. 5 IU daily) was commenced and continued for 14 days. The mice were killed 12 weeks following transplantation, and human ovarian grafts were retrieved.

Assessment of Follicular Development and Immunohistochemical Studies

For initial observations, ovarian grafts were observed following transplantation under a dissecting microscope. Transplanted grafts were fixed in 4% paraformaldehyde, cut into 3-μm thick sections, and mounted on a glass slide. Immunohistochemistry using streptavidin-biotin amplification (Histofine kit; Nichirei, Tokyo, Japan) was performed as previously described.[6] Polyclonal antibody for P450 cholesterol side chain cleavage (P450 scc) was kindly provided by Dr M. Okamoto (Osaka University School of Medicine, Osaka, Japan), and 3β-hydroxysteroid dehydrogenase (3β-HSD) polyclonal antibody was purchased from Oxygene (Dallas, TX, USA). P450 17α hydroxylase (P450 c17) polyclonal antibody was kindly provided by Dr J. I. Mason (University of Texas, Dallas, TX, USA), and polyclonal antibody for P450 aromatase (P450 arom) was kindly provided by Dr N. Harada (Fujita-Gakuen Health University, Toyoake, Japan). Estrogen receptor (ER) monoclonal antibody was purchased from Immunotech (ERID5; Marseilles, France). Ovarian follicles were classified based on the criteria of Clemont.[12]

Experiment 1

To evaluate the suitability of NOD-SCID and NOG mice as hosts for transplantation of human ovarian tissue, human ovarian cortex from four donors were transplanted into the back skin or ovarian bursa of NOD-SCID ($n = 10$) and NOG mice ($n = 10$). Before transplantation, bilateral ovariectomy was performed under anesthesia by dorsolateral laparotomy, and ovarian tissues were placed in each site. After transplantation, the ovarian bursa was closed by suturing with 9-0 nylon. No antibiotics were used. Ten weeks after transplantation, HMG was administered for 2 weeks, and the survival rates and development of human follicles were compared.

Experiment 2

The effect of transplantation site was determined by transplanting human ovarian tissue from four donors into the back skin, kidney capsule, and ovarian bursa of 25 NOG mice. Each mouse received two grafts in each of the three locations. Ten weeks after transplantation, HMG was administered for 2 weeks, and the survival rates and development of human follicles were compared.

Statistics

The chi-square test was applied to compare the number of follicles found in each graft sample. $P < 0.01$ was considered statistically significant.

Results

Experiment 1

Human ovarian tissue from four donors was transplanted in the back skin of NOD-SCID and NOG mice. Two pieces of donor tissue were transplanted into each mouse, with 10 host mice used for each strain. The tissue survival rate after transplantation was 80% (16/20) for NOD-SCID mice and 90% (18/20) for NOG mice. To examine whether follicle growth occurred in ovarian tissue transplanted into the back skin of NOD-SCID mice, the surviving grafts were sectioned and the central section of each graft was analyzed for follicular development. Five pre-antral follicles were observed in the sections taken from the 16 surviving grafts, and growth of follicles past the pre-antral stage was not observed. Grafts placed into the back skin of NOG mice were similarly analyzed. Five pre-antral follicles and five antral follicles with follicular cavities were observed in the sections taken from the 18 surviving grafts. Total number of antral follicle in the human ovarian tissue transplanted into NOG mice was significantly higher than that was transplanted into NOD-SCID mice (Table I).

Next, human ovarian tissue from four donors was transplanted in the ovarian bursa of NOD-SCID mice

American Journal of Reproductive Immunology 60 (2008) 534–540

Table I Survival and Follicular Development in the Human Ovarian Graft after Transplantation into the Back Skin of the Immunodeficient Mice

Mice strain (number of animals)	Ovarian grafts transplanted	Ovarian grafts survived*	Pre-antral follicle*	Antral follicle*
NOG	20	18[a]	5[b]	5[c]
NOD-SCID	20	16[a']	5[b']	0[c']

*The human ovarian tissue was examined after 2 weeks of human menopausal gonadotropin administration beginning 10 weeks after transplantation. Follicular growth was observed in a central section of a randomly selected graft.
a versus a', b versus b': not significant.
c versus c': $P < 0.05$.

Table II Survival and Follicular Development in the Human Ovarian Graft after Transplantation into the Kidney Capsule of the Immunodeficient Mice

Mice strain	Ovarian grafts transplanted	Ovarian grafts survived*	Pre-antral follicle*	Antral follicle*
NOG	20	18[a]	5[b]	4[c]
NOD-SCID	20	16[a']	4[b']	3[c']

*The human ovarian tissue was examined after 2 weeks of human menopausal gonadotropin administration beginning 10 weeks after transplantation. Follicular growth was observed in a central section of a randomly selected graft.
a versus a', b versus b', c versus c': not significant.

or NOG mice. Each of the 10 mice received two tissue grafts. The tissue survival rate after transplantation was 80% (16/20) in NOD-SCID mice and 90% (18/20) in NOG mice. To examine whether follicle growth occurred in ovarian tissue transplanted into the ovarian bursa of NOD-SCID mice, the surviving grafts were sectioned and the central section of each graft was analyzed for follicular development. Four pre-antral follicles and three follicles that had developed past the antral stage were observed in the sections taken from the 16 surviving grafts. Grafts transplanted into the ovarian bursa of NOG mice were similarly analyzed. Five pre-antral follicles and four antral follicles with follicular cavities were observed in the sections taken from the 18 surviving grafts. No significant difference was found in tissue survival rate and number of developed follicles between NOG mice and NOD-SCID mice (Table II).

Experiment 2

Human ovarian tissue from four donors was transplanted into NOG mice by placing two grafts into each of the following sites: the back skin, kidney capsule, and ovarian bursa. A total of 25 host NOG mice were used. Tissue survival rates after transplantation into NOG mice were 86% (43/50) in the back

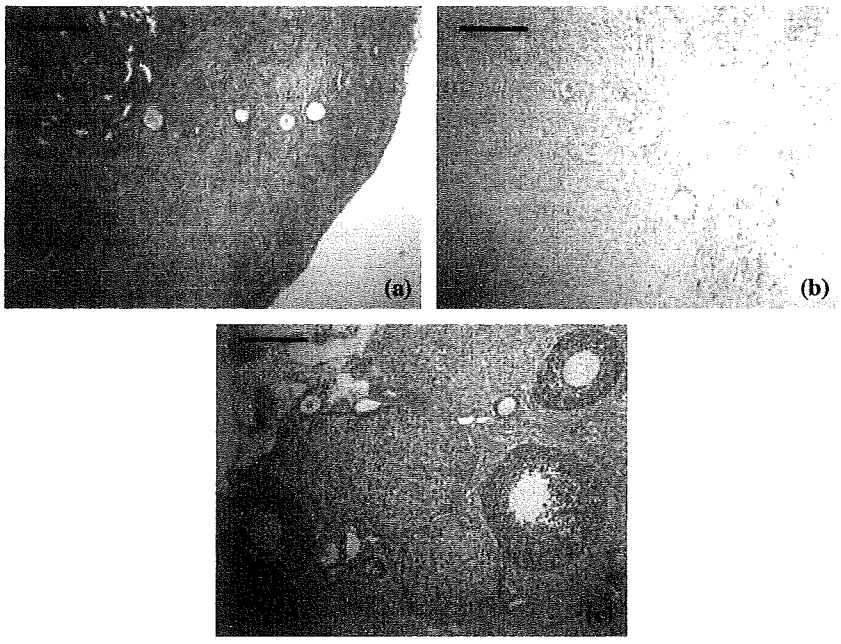

Fig. 1 Histology of human ovarian cortex grafts after transplantation into the back skin (a), kidney capsule (b), and ovarian bursa (c) of the same NOG mouse. More follicles developed in grafts placed in the ovarian bursa than in the back skin or kidney capsule. Scale bar = 200 μm.

Table III Survival and Follicular Development in the Human Ovarian Graft after Transplantation into Transplanted into Back Skin, Kidney Capsule and Ovarian Bursa of the Same NOG Mouse

Site of transplantation	Ovarian grafts transplanted	Ovarian grafts survived	Pre-antral follicle*	Antral follicle*	Graafian follicle*
Back skin	50	43^{a}	8^{b}	6^{c}	0^{d}
Kidney capsule	50	$44^{a'}$	$8^{b'}$	$5^{c'}$	$0^{d'}$
Ovarian bursa	50	$46^{a''}$	$23^{b''}$	$16^{c''}$	$2^{d''}$

*The human ovarian tissue was examined after 2 weeks of human menopausal gonadotropin administration beginning 10 weeks after transplantation. Follicular growth was observed in a central section of a randomly selected graft.
a versus a′ versus a″, b versus b′, c versus c′, d versus d′ versus d″: not significant.
b versus b″, b′ versus b″, c′ versus c″: $P < 0.01$.
c versus c″: $P < 0.05$.

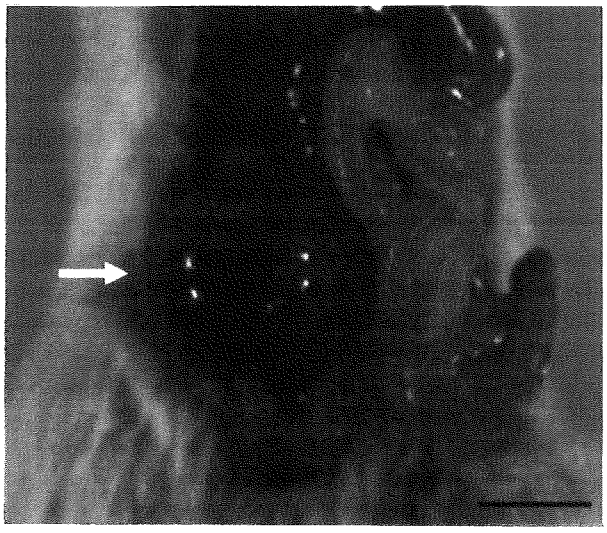

Fig. 2 Macroscopic view of a human Graafian follicle (arrow) after transplantation of human ovarian cortex into the ovarian bursa of a NOG mouse. Host mice were stimulated by daily intraperitoneal injection of human menopausal gonadotropin for 14 days, 10 weeks after transplantation. Scale bar = 1 cm.

skin, 88% (44/50) in the kidney capsule, and 92% (46/50) in the ovarian bursa. To determine whether follicle growth occurred in any of the grafts, they were sectioned and the central section of each graft was analyzed for follicular development (Fig. 1; summarized in Table III). Eight pre-antral follicles were observed in the sections taken from the 43 surviving grafts placed in the back skin, eight from the kidney capsule (out of 44 surviving grafts) and 23 in the ovarian bursa (out of 46 surviving grafts). Six antral follicles with follicular cavities were observed in the 43 surviving grafts placed in the back skin, five in the kidney capsule (out of 44 surviving grafts) and 16 in the ovarian bursa (out of 46 surviving grafts). The total number of human pre-antral and antral follicles developed in human ovarian tissue transplanted into ovarian bursa of NOG mice was significantly higher compared with the number of pre-antral and antral follicles developed in the back skin or kidney capsule of NOG mice (Table III). Graafian follicles (Fig. 2) were observed in two grafts in the ovarian bursa.

Immunohistochemistry

We next used immunohistochemistry to examine the expression of steroidogenic enzymes in human graft-derived Graafian follicles that developed in the ovarian bursa of NOG mice (Fig. 3). P450 scc, P450 c17 (data not shown), and 3β-HSD (data not shown) were localized in the theca cell layer and AD4BP was found in both theca and granulose cells. ER and P450 arom (data not shown) were also detected in the theca cell layer.

Discussion

NOG mice possess multiple immunological defects ranging from dysfunctional cytokine production to functional incompetence of T, B, and NK cells.[9] This combination of defects provides superb conditions for the development of a xenotransplanted graft. To compare the function as the host for xenotransplantation of human ovarian tissue, human ovarian cortex was transplanted into the back skin or ovarian bursa of NOG and NOD-SCID mice and the tissue survival rates and development of human follicles were

American Journal of Reproductive Immunology 60 (2008) 534–540

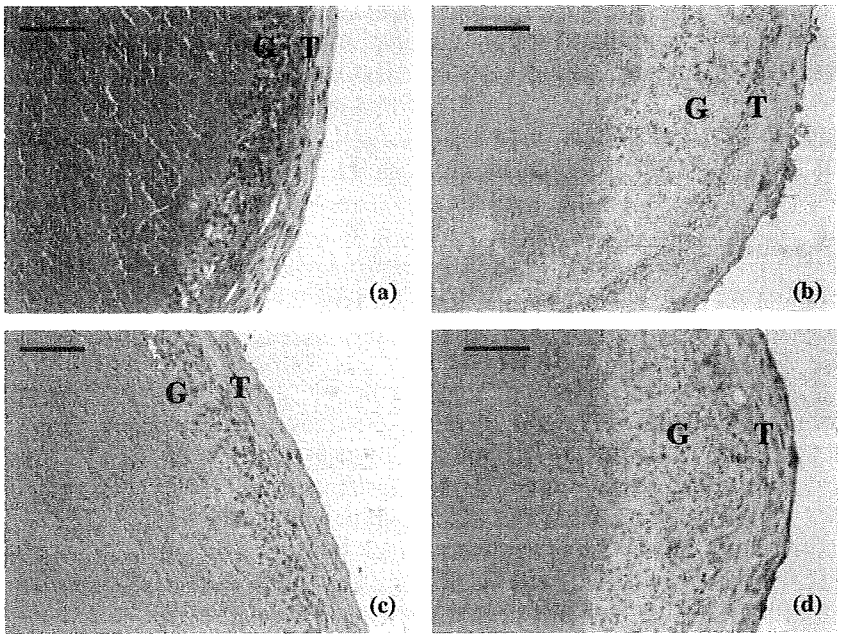

Fig. 3 Characterization of a human Graafian follicle that developed in the ovarian bursa of a NOG mouse (same follicle as shown in Fig. 1). (a) Hematoxylin and eosin staining showing the theca and granulosa cell layers. (b) Antibody staining for the steroidogenic enzyme P450 scc is localized to the cytoplasm of theca cells. (c) Immunohistochemistry for AD4-BP showing expression in the nuclei of both theca and granulosa cell layers. (d) ER antibody staining was detected in the theca cell layer. T, theca cells; G, granulosa cells. Scale bar = 100 μm.

compared. Grafts placed in the ovarian bursa and back skin of NOG mice both showed approximately similar survival rates after transplantation and formed more pre-antral to antral follicles as did ovarian tissue transplantated into NOD-SCID mice (Tables I and II). Development of mature human Graafian follicles (as shown in Fig. 2) was only observed in human ovarian tissue transplanted into the ovarian bursa of NOG mice. From these results, we conclude that NOG mice are better than NOD-SCID mice as a host strain for human ovarian xenografting.

We also examined how the site of transplantation affects the survival rate and follicular development in human ovarian tissue grafted into NOG mice. When human ovarian cortex was transplanted into the back skin, kidney capsule, and ovarian bursa of NOG mice, the most pre-antral or antral follicles developed in the human ovarian tissue, which were transplanted into mices' ovarian bursa. Moreover, in two out of eight transplanted mice, human Graafian follicles (16–18 mm in diameter) were obtained from transplanted tissues within the ovarian bursa (Fig. 2). In contrast, while antral follicles were found in grafts into the back skin or kidney capsule, no Graafian follicles were observed. Thus, the mouse ovarian bursa provides a good microenvironment (e.g. blood flow, kinetics of exogenous gonadotropins, growth factors) for follicular growth and differentiation of grafted human ovarian tissue. However, the reasons for this improved follicular growth and differentiation are still unclear. Interestingly, only one Graafian follicle was formed per graft, suggesting that the mouse ovarian bursa may supply environmental conditions that support the development of single follicles.

We also examined the expression of steroidogenic enzymes in graft-derived follicles by immunohistochemistry. High levels of P450 arom and ER expression were observed in both the granulosa and the theca layer in grafts into the ovarian bursa of NOG mice. The steroidogenic enzymes P450 scc, P450 c17, and 3β-HSD were observed in the cytoplasm of theca cells in antral follicles following xenotransplantation into both NOD-SCID[6] and NOG mice (present study). P450 arom and ER are expressed specifically in Graafian follicles in cycling human ovaries and mark the completion of steroidogenesis in human follicles,[13–15] whereas estrogen plays dual roles in folliculogenesis (via an autocrine system) and oocyte cytoplasmic maturation.[16] P450 arom and ER expression were observed only in the granulosa and theca cell layer in human Graafian follicles that formed in the ovarian bursa of NOG mice (Fig. 3). Thus, the follicles we observed have characteristics similar to the dominant follicles of a normal, pre-menopausal cycling human ovary.

In summary, we have found that NOG mice are good hosts for xenotransplantation of the human

ovarian cortex and that tissue survival and follicle growth vary with the site of transplantation. Our data provide the biological evidence that Graafian follicles can develop outside the human body. This system will allow us to elucidate the mechanisms of human follicular development, which remain elusive.

Acknowledgment

This work was supported by Japan Society for the Promotion of Science to Y.T.

References

1 Gook DA, Edgar DH, Borg J, Archer J, McBain JC: Diagnostic assessment of the developmental potential of human cryopreserved ovarian tissue from multiple patients using xenografting. *Human Reprod* 2005; 20:72–78.
2 Aubard Y: Ovarian tissue xenografting. *Eur J Obstet Gynecol Reprod Biol* 2003; 108:14–18.
3 Shultz LD, Ishikawa F, Greiner DL: Humanized mice in translational biomedical research. *Nat Rev Immunol* 2007; 7:118–130.
4 Weissman A, Gotlieb L, Colgan T, Jurisicova A, Greenblatt EM, Casper RF: Preliminary experience with subcutaneous human ovarian cortex transplantation in the NOD-SCID mouse. *Biol Reprod* 1999; 60:1462–1467.
5 Gook DA, Edgar DH, Borg J, Archer J, Lutjen PJ, McBain JC: Oocyte maturation, follicle rupture and luteinization in human cryopreserved ovarian tissue following xenografting. *Hum Reprod* 2003; 18:1772–1781.
6 Sato Y, Terada Y, Utsunomiya H, Koyanagi Y, Ito M, Miyoshi I, Suzuki T, Sasano H, Murakami T, Yaegashi N, Okamura K: Immnohistochemical localization of steroidogenic enzymes in human follicle following xenotransplantation of the human ovarian cortex into NOD-SCID mice. *Mol Reprod Dev* 2003; 65:67–72.
7 Hovatta O, Wright C, Krausz T, Hardy K, Winston RM: Human primordial, primary and secondary ovarian follicles in long-term culture: effect of partial isolation. *Hum Reprod* 1999; 14:2519–2524.
8 West ER, Shea LD, Woodruff TK: Engineering the follicle microenvironment. *Semin Reprod Med* 2007; 25:287–299.
9 Ito M, Hiramatsu H, Kobayashi K, Suzue K, Kawahata M, Hioki K, Ueyama Y, Koyanagi Y, Sugamura K, Tsuji K, Heike T, Nakahata T: NOD/SCID/gamma(c)(null) mouse: an excellent recipient mouse model for engraftment of human cells. *Blood* 2002; 100:3175–3182.
10 Miyakawa Y, Ohnishi Y, Tomisawa M, Monnai M, Kohmura K, Ueyama Y, Ito M, Ikeda Y, Kizaki M, Nakamura M: Establishment of a new model of human multiple myeloma using NOD/SCID/gammac(null) (NOG) mice. *Biochem Biophys Res Commun* 2004; 313:258–262.
11 Donnez J, Dolmans MM, Demylle D, Jadoul P, Pirard C, Squifflet J, Martinez-Madrid B, van Langendonckt A: Livebirth after orthotopic transplantation of cryopreserved ovarian tissue. *Lancet* 2004; 364:1405–1410.
12 Clement PB: Histology of the ovary. *Am J Surg Pathol* 1987; 11:277–303.
13 Sasano H, Okamoto M, Mason JI, Simpson ER, Mendelson CR, Sasano N, Silverberg SG: Immunolocalization of aromatase, 17α-hydroxylase and side-chain-cleavage cytochromes P-450 in the human ovary. *J Reprod Fertil* 1989; 85:163–169.
14 Suzuki T, Sasano H, Tamura M, Aoki H, Fukaya T, Yajima A, Nagura H, Mason JI: Temporal and spatial localization of steroidogenic enzymes in premenopausal human ovaries: in situ hybridization and immunohistochemical study. *Mol Cell Endocrinol* 1993; 97:135–143.
15 Suzuki T, Sasano H, Kimura N, Tamura M, Fukaya T, Yajima A, Nagura H: Immunohistochemical distribution of progesterone, androgen and oestrogen receptors in the human ovary steroidogenic enzymes. *Hum Reprod* 1998; 13:1922–1927.
16 Tesarik J, Mendoza C: Nongenomic effects of 17 beta-estradiol on maturing human oocytes: relationship to oocyte developmental potential. *J Clin Endocrinol Metab* 1995; 80:1438–1443.

American Journal of Reproductive Immunology **60** (2008) 534–540

Exp. Anim. 57(5), 471–477, 2008

—Note—

Establishing EGFP Congenic Mice in a NOD/Shi-scid IL2Rg^{null} (NOG) Genetic Background Using a Marker-Assisted Selection Protocol (MASP)

Hiroshi SUEMIZU, Chie YAGIHASHI, Tomoko MIZUSHIMA, Tomoyuki OGURA, Tomoo ETOH, Kenji KAWAI, and Mamoru ITO

Central Institute for Experimental Animals, 1430 Nogawa, Miyamae, Kawasaki 216-0001, Japan

Abstract: *Severely immunocompromised NOD/Shi-scid IL2Rg^{null} (NOG) mice, which show higher engraftment efficiency, are useful as recipients in xenotransplantation studies. We generated a NOG-enhanced green fluorescent protein (EGFP) transgenic (Tg) mouse (NOG-EGFP) that was introduced the EGFP transgene from the C57BL/6-EGFP Tg mouse using the speed congenic method with a marker-assisted selection protocol (MASP). With this method, the selection of the male with the closest NOG strain type was repeated four times. When human cord blood CD34$^+$ cells were transplanted into NOD/Shi-scid, NOG, and NOG-EGFP mice (N_6), the engraftment efficiency of the NOG-EGFP mice was significantly higher than that of the NOD/Shi-scid mice and was similar to that of the NOG mice. These results suggest that the NOG-EGFP mice, which were generated using the congenic method with MASP, acquired the immunological properties of the NOG mice.*

Key words: *microsatellite marker, NOG mouse, speed congenic*

Previously established techniques of introducing additional genetic changes into transgenic or knockout mice include transgenic methods involving the direct microinjection of fertilized eggs and congenic strategies using extant genetically modified mice. The congenic strategy is the classical method and is easiest to perform, but, backcrossing must be performed for at least seven generations to replace over 99% of the genetic background (99.2% is theoretically replaced), which is extremely time-consuming. One of the fastest ways to introduce additional genetic modification is the marker-assisted selection protocol (MASP) known as the "speed congenic" method. In MASP, the male mouse showing the most complete replacement with the targeted genetic background is selected as the "best" male and is used in the next backcross [11–13]. NOG (formally, NOD.Cg-*Prkdc^{scid} Il2rg^{tm1Sug}*/ShiJic) mice, which were developed by introducing IL2Rg^{null} mutation from C57BL/6-*Il2rg^{tm1Sug}* mice with backcross mating to NOD/Shi-*scid* mice [3], have no lymphocytes (neither T nor B) or natural killer (NK) cells, and have impaired dendritic cell function [4, 7]. Therefore, NOG mice can be used to develop "humanized mice", which possess high levels of human-derived cells or tissues. Because it is difficult to label human cells (e.g. hematopoietic stem cells or neural stem cells) with visible markers, we

(Received 26 July 2007 / Accepted 21 April 2008)

Address corresponding: H. Suemizu, Central Institute for Experimental Animals, 1430 Nogawa, Miyamae, Kawasaki 216-0001, Japan

attempted to introduce the enhanced green fluorescent protein (EGFP) gene into the NOG mouse as a visible recipient marker, which if successful would make it easier to differentiate donor cells from recipient cells in studies of transplantation and regenerative medicine.

This study was performed in accordance with institutional guidelines and was approved by the Animal Experimentation Committee of the Central Institute for Experimental Animals. NOG mice expressing the EGFP gene can be obtained reliably by backcrossing with an animal in which the phenotype of the modified gene is already expressed in the donor. Therefore, we mated an inbred line of C57BL/6-*Tg(Act-EGFP)C14-Y01-FM1310sb* (C57BL/6-TgEGFP) mice [6, 8] with a NOG mice to make a NOG-EGFP (NOD.Cg-*Prkdc*^{scid} *Il2rg*^{tm1Sug} *Tg(Act-EGFP)C14-Y01-FM1310sb*/ShiJic) mice. Tail clips of the mice were obtained and digested with proteinase K using standard methods [9]. Genomic DNA was extracted using the MagExtractor System MFX-9600 Magnia R Plus (Toyobo, Osaka, Japan) according to the manufacturer's instructions. The EGFP transgene was genotyped by PCR with the forward primer GFP-F1 (5'-CTGGTCGAGCTGGACGGCGACG-3') and reverse primer GFP-R1 (5'-CACGAACTCCAGCAGGACCATG-3'). The *scid* and IL2Rg^{null} mutations were genotyped using a previously described PCR method [2, 3]. Three to six microsatellite markers were selected from each chromosome, including the X-chromosome. We selected 87 microsatellite markers to evaluate the mouse genetic backgrounds of the C57BL/6, NOG, and 129S6/SvEv strains because the Tg EGFP mice originated in C57BL/6, and the IL2Rg^{null} mutants were generated with mouse ES cells (CCE) derived from the 129S6/SvEv strain. To evaluate the genetic background in more detail, an additional 17 microsatellite markers were arranged on chromosome 9. General information about the primers, including the size of the PCR product, is listed in Table 1. First, 10–100 ng of genomic DNA was suspended in a total volume of 12.5 μl PCR buffer containing 20 mM Tris-HCl (pH 8.4), 50 mM KCl, 1.5 mM $MgCl_2$, 0.1–0.3 μM fluorescence-labeled primers, 0.2 mM dNTP, and 1.0 unit of Platinum GenoType *Tsp* DNA polymerase (Invitrogen, Carlsbad, CA, USA). Using a Bio-Rad iCycler (Bio-Rad Laboratories, Hercules, CA, USA), the thermal cycling conditions consisted of 1 cycle at 95°C for 2 min followed by: 10 cycles at 94°C for 45 s, 60°C for 1 min, and 72°C for 1 min; then, 17 cycles at 89°C for 1 min, 60°C for 1 min, and 72°C for 1 min; with a final extension of 10 min at 72°C. Following PCR, 2 μl of product, 0.6 μl of GS500-LIZ size standard (Applied Biosystems, Foster City, CA, USA), and 24.4 μl of Hi-Di formamide (Applied Biosystems) were mixed and denatured at 95°C for 2 min, cooled on ice, and then loaded directly on an ABI 3130xl Genetic Analyzer (Applied Biosystems). The electrophoresis data were processed using GeneMapper 4.0 software (Applied Biosystems). When non-labeled primer pairs were used, the PCR products were electrophoresed on 3% NuSieve 3:1 agarose (Lonza Walkersville, Inc., Walkersville, MD, USA) gel/20 mM Tris-acetate, 2.5 mM EDTA (0.5 × TAE) and then stained with ethidium bromide (0.25 μg/ml). Statistical analyses were performed with StatView 5.0 and Prism 5 software.

To introduce the EGFP transgene into NOG mice, the first generation hybrid (F_1) was obtained by mating a male C57BL/6-TgEGFP mouse as the donor with a recipient NOG female mouse. The F_1 hybrid received a uniform genome (except for the sex chromosome) from the donor and recipient, and the replacement rate (described as "% Recipient genome" in Table 2) for both the expected and observed values was 50% (Table 2). In the next stage, a randomly selected male F_1 mouse with the EGFP transgene was again mated with female NOG recipient mice to obtain the N_2 generation. Marker-assisted selection was started at the N_2 generation to select the "best" male congenic mouse. Using the 61 informative markers, the male with the closest NOG strain type was selected as the parent for the N_3 generation. Using this method, the selection of males with the closest NOG strain type was repeated four times. The observed "% Recipient genome" of the male closest to the NOG background was 81.1, 95.9, 98.4, and 99.2% in the N_2, N_3, N_4, and N_5 generations, respectively. The higher values of the observed "% Recipient genome" in generation N_3 and N_4 were statistically significant (P=0.018 and 0.067, respectively, Fisher's exact probability test). Wakeland *et al.* described the rationale of speed congenics, and stated that the advantage of screening with low-density markers (25 cM marker spacing) was realized in the N_3 and N_4 generations [12]. Com-

Table 1. MASP primer pairs and PCR product sizes in the NOG, C57BL/6, and 129S6/SvEv strains

Marker	Position (cM) [b]	NOG	C57BL/6	129S6/SvEv (CCE ES)	Dye	Marker	Position (cM) [b]	NOG	C57BL/6	129S6/SvEv (CCE ES)	Dye
D1Mit67 [a]	9	125	133	125	NED	*D9Mit182*	55	115	99	104	NL [c]
D1Mit303	34.8	112	122	112	NED	*D9Mit53*	57	198	206	198	FAM
D1Mit132 [a]	43.1	160	141	160	NED	*D9Mit184*	60	125	132	127	FAM
D1Mit91	64	146	146	138	PET	*D9Mit20*	61	95	104	114	FAM
D1Mit102 [a]	73	121	110	125	FAM	*D9Mit214*	62	135	137	108	FAM
D1Mit459 [a]	102	116	120	116	PET	*D9Mit215*	63	116	116	122	NED
D2Mit1 [a]	1	111	115	113	VIC	*D9Mit281*	68	106	111	106	FAM
D2Mit312	1	120	120	111	PET	*D9Mit120*	69	126	146	146	NL [c]
D2Mit182 [a]	38.3	149	153	149	PET	*D9Mit52* [a]	72	173	171	171	VIC
D2Mit311 [a]	83.1	110	121	115	VIC	*D10Mit2* *[a]	16	133	126	133	NED
D2Mit346 [a]	91.8	107	101	118	PET	*D10Mit31* [a]	36	146	148	151	NED
D3Mit149 *[a]	2.4	147	138	138	PET	*D10Mit266* [a]	62	82	90	84	PET
D3Mit62	4.6	117	117	110	NED	*D11Mit21* [a]	20	147	158	147	VIC
D3Mit25 [a]	29.5	127	129	123	VIC	*D11Mit67* [a]	57	133	131	122	VIC
D3Mit85 [a]	72.9	226	218	224	VIC	*D11Mit48* [a]	77	123	129	123	NED
D3Mit89 [a]	86.1	214	220	214	FAM	*D11Mit184*	78	ND	149	160	NED
D4Mit227 [a]	3.2	182	180	172	VIC	*D12Mit109* [a]	19	124	116	124	VIC
D4Mit52 [a]	54.9	110	119	112	PET	*D12Mit156* [a]	34	184	176	171	FAM
D4Mit190	79	ND	138	130	FAM	*D12Mit30*	46	103	103	113	PET
D4Mit256 [a]	82.7	128	132	128	FAM	*D12Mit133* [a]	56	96	111	111	FAM
D5Mit146 [a]	1	125	120	115	PET	*D13Mit132* [a]	4	157	150	157	NED
D5Mit1	5	135	135	129	VIC	*D13Mit13* [a]	35	145	151	145	PET
D5Mit58 [a]	41	116	114	123	NED	*D13Mit51* [a]	59	139	137	130	FAM
D5Mit367 [a]	65	96	102	92	FAM	*D14Mit1* [a]	3	101	104	98	PET
D5Mit97 [a]	74	118	124	118	NED	*D14Mit233* [a]	19.5	182	194	179	VIC
D6Mit86 [a]	0.5	121	132	121	NED	*D14Mit225* [a]	42.5	94	111	102	FAM
D6Mit284 [a]	37.5	129	138	129	FAM	*D15Mit12*	4.7	143	143	151	FAM
D6Mit304 [a]	75	105	115	107	PET	*D15Mit13* [a]	6.7	138	133	116	NED
D7Mit267 [a]	11	174	187	199	VIC	*D15Mit85*	16.4	194	194	199	FAM
D7Mit193	24.5	149	149	159	VIC	*D15Mit171* [a]	54.5	141	132	141	FAM
D7Mit350 [a]	41	138	116	122	FAM	*D15Mit42* [a]	59.2	178	182	159	VIC
D7Mit100	53.5	201	201	193	VIC	*D16Mit129* *[a]	3.4	161	180	167	PET
D7Mit189 [a]	72.4	114	129	114	PET	*D16Mit139* [a]	43.1	150	144	170	VIC
D8Mit155 *[a]	1	156	161	108	NED	*D16Mit48*	43.3	155	155	159	VIC
D8Mit217	6	169	169	179	FAM	*D16Mit106* [a]	71.5	132	142	132	PET
D8Mit191 [a]	21	122	133	122	VIC	*D17Mit163* [a]	3	126	130	124	VIC
D8Mit88 [a]	58	127	114	114	PET	*D17Mit138*	24.2	ND	138	129	FAM
D8Mit93	72	169	169	163	NED	*D17Mit53* [a]	38.5	122	128	122	VIC
D9Mit250	5	123	123	132	VIC	*D17Mit93* [a]	44.5	141	154	141	NED
D9Mit83 [a]	6	129	134	134	PET	*D18Mit19*	2	150	150	133	FAM
D9Mit97 [a]	29	162	151	159	VIC	*D18Mit12* [a]	17	122	110	110	FAM
D9Mit102	31	144	140	144	FAM	*D18Mit91* [a]	29	135	137	137	PET
D9Mit207	33	160	148	155	NL [c]	*D18Mit40*	37	135	137	137	FAM
D9Mit105	35	116	145	145	NL [c]	*D18Mit187* [a]	47	106	110	110	FAM
D9Mit259	38	122	112	115	NL [c]	*D18Mit25*	57	117	117	109	NED
D9Mit107	40	119	120	104	FAM	*D19Mit78* [a]	5	130	126	128	FAM
D9Mit8	42	185	178	169	VIC	*D19Mit14* [a]	15	150	153	146	PET
D9Mit124	42	128	124	124	FAM	*D19Mit103* [a]	52	117	115	123	NED
D9Mit236	43	125	143	125	NL [c]	*DXMit55* [a]	1.4	121	129	127	NED
D9Mit11	48	112	74	100	NL [c]	*DXMit25* [a]	27.8	158	168	158	VIC
D9Mit275	50	115	110	110	FAM	*DXMit130*	55	161	161	136	VIC
D9Mit35	52	112	124	124	NL [c]	*DXMit121* [a]	67	130	147	147	VIC

[a]: Informative microsatellite markers for distinguishing between the NOG and C57BL/6 strains; [b]: according to the Mouse Genome Database (MGD; http://www.informatics.jax.org); *: Primers were changed from the original sequence on the NCBI UniSTS database to redesigned sequences in order to change the size of the PCR product as follows; *D3Mit149*: F 5'-TTCCATACAAACAAAAGCAACG-3', R 5'-CTATATAGCTGTAAATGTAAAGTGTATGTC-3', *D8Mit155*: F 5'-TTGGACAGGGAAAATTCTGC-3', R 5'-GAAAATGTGACACCATTTGAGGAC-3', *D10Mit2*: F 5'-GTTCATTTGAGGCACAAGCA-3', R 5'-TTTGAGCTGCTCACAACCC-3', and *D16Mit129*: F 5'-ATGAGCAGTCTGCAGACCTT-3', R 5'-GAGACTGAGAAAGGGGATGC-3'; [c]: non-labeled primer pairs; ND: not detected.

Table 2. Comparison of the methods used to generate NOG-EGFP mice

Generation number[a] (Number examined[b])	% Recipient genome (R/total)[c]			
	Expected	Observed		
		MAX	MIN	AVG ± SD
P	0	–	–	–
F_1	50 (61/122)	50 (61/122)	–	–
N_2 (13)	75 (91.5/122)	81.1 (99/122)	66.4 (81/122)	73.1 ± 4.1
N_3 (15)	87.5 (106.8/122)	95.9 (117/122) *	88.5 (108/122)	91.3 ± 2.4
N_4 (31)	93.8 (114.4/122)	98.4 (120/122) **	95.9 (117/122)	96.9 ± 0.8
N_5 (4)	96.9 (118.2/122)	99.2 (121/122)	98.4 (120/122)	98.8 ± 0.5

[a]The generation count begins at strain P (parental) defined as 100% original background, 0% recipient background. The F_1 generation contains the offspring from the intercross between P (100% original) × pure recipient NOG strains (100% recipient). F_1 animals have 50% of the recipient genome. [b]The numbers of transgenic male mice whose genetic backgrounds were examined. [c]R: the number of homozygotes for the allele of the recipient strain; total: total number of alleles. *P=0.015 and **P=0.095 (Fisher's exact probability test).

puter simulations of MASP-based congenic strain construction strategies using high-density (10 cM apart) and low-density (25 cM apart) marker spacing, and screening a mean of 40 and 16 progeny per generation revealed that screening 16 progeny per generation with a low-density marker was the most cost-effective strategy. Our MASP strategy is similar to the computer-simulated most cost-effective strategy because 61 informative microsatellite markers were arranged throughout the mouse genome spaced at an average distance of 26.5 cM (low density), and we screened 13, 15, and 31 progeny at N_2, N_3, and N_4, respectively. However, our MASP strategy included some gaps of over 30 cM, with a largest gap of 51.7 cM. One major problem is that a larger gap might not be able to detect a double crossing-over occurring in meiosis. Hameister *et al.* examined the frequency of double crossing-over in a 55.4-cM region between chromosome 15A2 and 15F2-3 in 151 mice and found only one animal with a double crossing-over [2]. In reality, double crossing-over does not occur at a high frequency, even in a larger gap extending over 50 cM. Therefore, detecting double crossing-over using adjacent markers might be possible. Another problem is the inability to detect a small segment of the donor genome. Because screening all gaps over 30 cM is unrealistic, we screened one large gap (43 cM) extending between *D9Mit97* and *D9Mit52* in more detail. We used extremely high-density markers (2.4 cM marker spacing) consisting of 17 informative markers in 12 and 14 progeny at N_2 and N_3, respectively. No animal with a double crossing-over was found in 12 animals in the N_2 generation, while a small contaminating segment of the donor genome was detected between markers *D9Mit207* and *D9Mit107* in progeny #E109 of the N_3 generation (Fig. 1). Considering an undetected contaminating donor genome, Wakeland *et al.* recommended performing one or two additional backcrosses when all of the markers become recipient-derived. This additional backcross reduces the level of undetected contamination in these strains to the equivalent of that at N_{10} or N_{11} using the traditional protocol [12]. When transferring a transgene or modified gene into the NOG or C57BL/6 strain from C57BL/6 or NOG and 129S6/SvEv backgrounds, our selected 61 markers serve as genetic quality standards for generating a congenic strain using MASP. The final backcross could be completed because the NOG-EGFP mouse (N_5) met the genetic quality standards after backcrossing four times. However, we persisted with backcrossing during the production of congenic progeny derived from the N_5 generation for xenotransplantation studies. This additional backcross might confer some benefit through the further elimination of residual donor genomes.

To examine the phenotype of the NOG-EGFP mice, the male mouse closest to the NOG strain with EGFP transgene in the N_5 generation was mated with female NOG mice to obtain many NOG-EGFP mice (N_6) for xenotransplantation studies. NOD/Shi-*scid* mice (male, 10 weeks old), NOG mice (female, 7 weeks old), and NOG-EGFP mice (female, 12 weeks old) were irradiated with 2.4 Gy of X-rays 24 h before transplanting 5

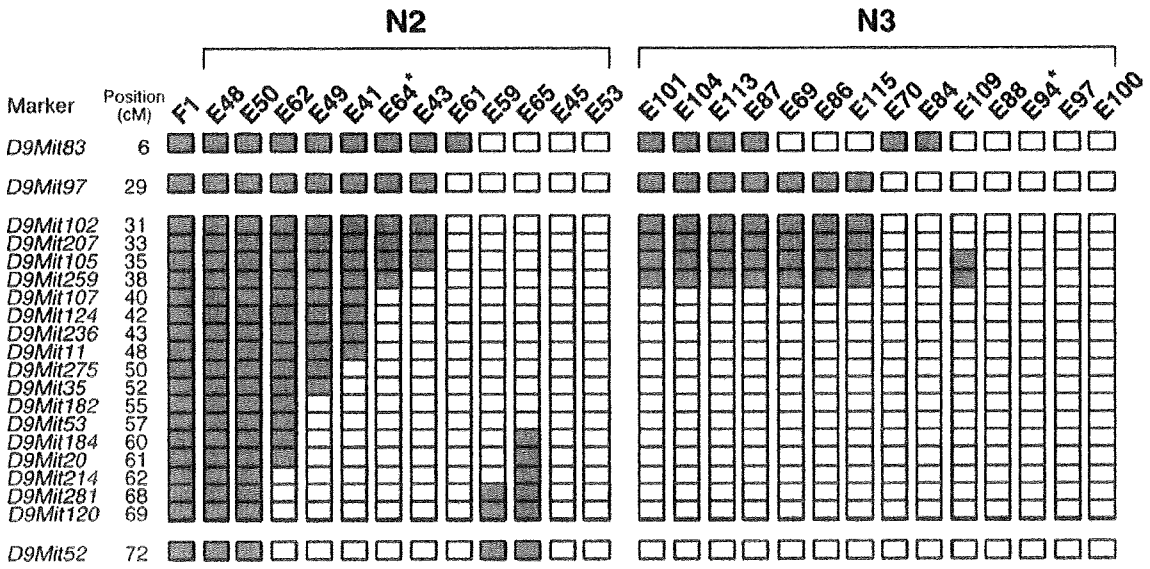

Fig. 1. Detailed screening between *D9Mit97* and *D9Mit52* using extremely high-density markers (2.4 cM marker spacing). The screening is depicted schematically using genotyping data in which each box indicates one informative microsatellite marker primer pair. The yellow boxes represent those PCR products that are identified as NOG homozygotes based on size. The red boxes represent C57BL/6 and NOG heterozygotes. The asterisks indicate the "best" males that were selected as the parents of the next backcross generation.

$\times 10^4$ human CD34$^+$ cells (Lonza Walkersville, Inc.). The engraftment of donor cells was monitored every 4 weeks by detecting the human cells expressing the leukocyte common Ag CD45 (Immunotech, Marseille, France) using a MoFlo flow cytometer (Dako, Glostrup, Denmark) and Summit software. Representative flow cytometric analysis of peripheral blood of mice that underwent transplantation (after 12 weeks) is shown in Fig. 2a. When using NOG-EGFP mice as recipients, we could easily differentiate donor human cells from recipient mouse cells with the fluorescent signals of the EGFP, although the cells were not stained with any cell surface marker for the mouse species. Twelve weeks after transplantation, significantly more growth of human cells was observed in both NOG mice and NOG-EGFP mice compared to NOD/Shi-*scid* mice ($^*P<0.01$; $^{**}P<0.001$; Fig. 2b), but there was no significant difference between NOG mice and NOG-EGFP mice. These results suggest that the NOG-EGFP mice, which were generated by the congenic method with MASP, acquired the immunological properties of the NOG strain.

In this experiment, we did not use X-chromosome-derived microsatellite markers as informative markers to select a parent for the next generation because the X-chromosome is always derived from the recipient NOG strain in male transgenic mice. However, we checked the X-chromosome with informative markers to distinguish between the NOG and 129S6/SvEv strains (the source of the CCE ES cells) because of the confirmation of an X-chromosome linked IL2Rg^{null} mutation (Chr X, 38 cM) derived from the recipient genome. However, the nearest marker located at 32.1 cM was not informative, and the other three markers on the X-chromosome were shown to be homozygous for recipient-derived alleles.

Nakanishi *et al.* analyzed transgene integration sites in more than 100 EGFP transgenic mouse lines rigorously using fluorescent *in situ* hybridization and determined that the EGFP transgene is located on the D1 region of chromosome 14 in the 131 line (C57BL/6-*Tg (Act-EGFP) C14-Y01-FM1310sb*) [6]. The microsatellite markers that did not become NOG markers in the N_4 generation were the markers *D14Mit233* and *D14Mit225*, both of which are on chromosome 14. Fortunately, we could change the genetic background around the *D14Mit225* region from C57BL/6 to the NOG strain in the N_5 generation, but the genetic background around the *D14Mit233* region remained C57BL/6. *D14Mit233*

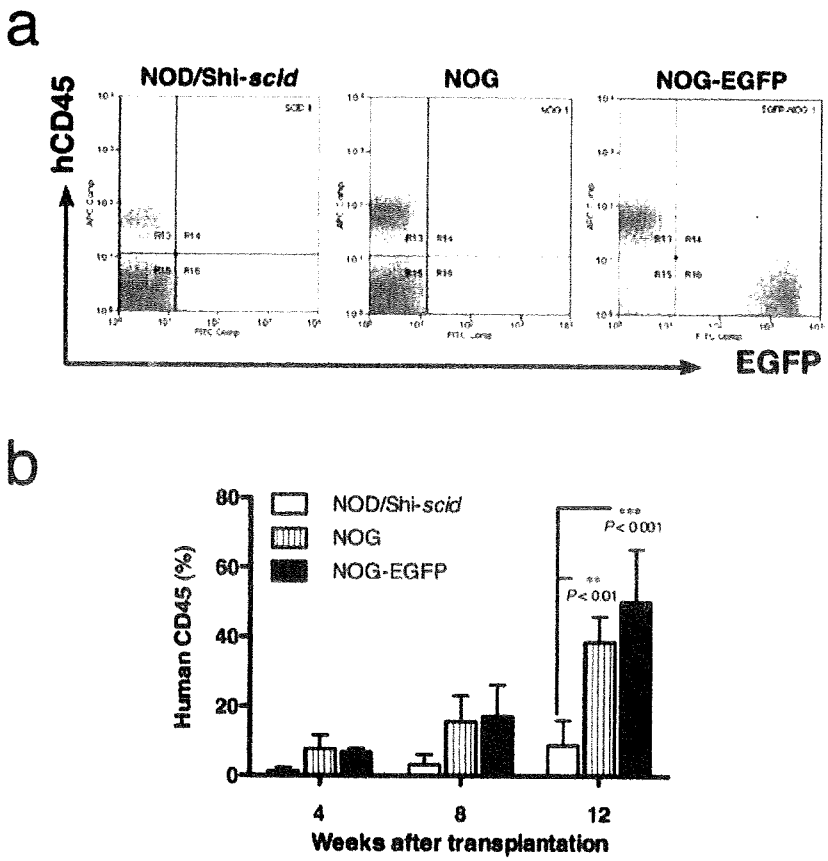

Fig. 2. High engraftment efficiency of human cells in NOG-EGFP mice. (a) Representative flow cytometric data for peripheral blood obtained from NOG-EGFP mice that underwent human cord blood $CD34^+$ cell transplantation (12 weeks after transplantation). (b) Comparison of the engraftment levels of human cells in NOD/Shi-*scid*, NOG, and NOG-EGFP mice. At the indicated times following transplantation of 5×10^4 $CD34^+$ cells, human $CD45^+$ cells in mouse peripheral blood were assayed by flow cytometry (n=3 each). $^{**}P<0.01$, $^{***}P<0.001$.

and *D14Mit225* are located in the B and D1–D3 regions, respectively. These markers are located extremely close to the site of EGFP transgene integration in the C5BL/6-TgEGFP line 131. The *D14Mit233* marker seemed to be closer to the integrated transgene than the *D14Mit225* marker because six recombinants at the *D14Mit225* locus were observed in the 63 male Tg EGFP mice, while no recombinant was observed for the *D14Mit233* marker. The distance from the *D14Mit225* marker to the integrated EGFP transgene can be calculated as roughly 9.5 cM based on the recombination frequency [10]. Based on statistical modeling, the traditional 12 backcross generation (N_{12}) protocol will produce a congenic strain in which more than 99% of the genome is unlinked to the target gene carried in a donor-derived genome segment with an average length of about 20 cM [1]. Therefore, the *D14Mit233* marker genetically linked to the transgene integration site is physically close enough to the transgene that it will not segregate independently during meiosis.

Acknowledgment(s)

We thank Noriko Omi and Chika Kito of CIEA for their technical assistance and Dr. Masaru Okabe (Osaka University) for providing the green mice.

References

1. Flaherty, L. 1981. pp. 215–221. *In*: The Mouse in Biomedical Research: History, Genetics, and Wild Mice, Vol. 1. (Foster, H.L., Small, J.D., and Fox, J.G., eds.), Academic Press, New York.
2. Hameister, H., Schulz, W.A., Meyer, J., Thoma, S., Adolph, S., Gaa, A., and von Deimling, O. 1992. *Genomics* 14: 417–422.
3. Ito, M., Hiramatsu, H., Kobayashi, K., Suzue, K., Kawahata, M., Hioki, K., Ueyama, Y., Koyanagi, Y., Sugamura, K., Tsuji, K., Heike, T., and Nakahata, T. 2002. *Blood* 100: 3175–3182.
4. Koyanagi, Y., Tanaka, Y., Kira, J., Ito, M., Hioki, K., Misawa, N., Kawano, Y., Yamasaki, K., Tanaka, R., Suzuki, Y., Ueyama, Y., Terada, E., Tanaka, T., Miyasaka, M., Kobayashi, T., Kumazawa, Y., and Yamamoto, N. 1997. *J. Virol.* 71: 2417–2424.
5. Maruyama, C., Suemizu, H., Tamamushi, S., Kimoto, S., Tamaoki, N., and Ohnishi, Y. 2002. *Exp. Anim.* 51: 391–393.
6. Nakanishi, T., Kuroiwa, A., Yamada, S., Isotani, A., Yamashita, A., Tairaka, A., Hayashi, T., Takagi, T., Ikawa, M., Matsuda, Y., and Okabe, M. 2002. *Genomics* 80: 564–574.
7. Ohbo, K., Suda, T., Hashiyama, M., Mantani, A., Ikebe, M., Miyakawa, K., Moriyama, M., Nakamura, M., Katsuki, M., Takahashi, K., Yamamura, K., and Sugamura, K. 1996. *Blood* 87: 956–967.
8. Okabe, M., Ikawa, M., Kominami, K., Nakanishi, T., and Nishimune, Y. 1997. *FEBS Lett.* 407: 313–319.
9. Sambrook, J. and Russell, D.W. 2001. Molecular Cloning, Third Edition: A Laboratory Manual. Cold Spring Harbor Laboratory Press, New York.
10. Sturtevant, A.H. 1913. *J. Exp. Zool.* 14: 43–59.
11. Teppner, I., Aigner, B., Schreiner, E., Müller, M., and Windisch, M. 2004. *Lab. Anim.* 38: 406–412.
12. Wakeland, E., Morel, L., Achey, K., Yui, M., and Longmate, J. 1997. *Immunol. Today* 18: 472–477.
13. Wong, G.T. 2002. *Neuropeptides* 36: 230–236.

Biochemical and Biophysical Research Communications 377 (2008) 248–252

Contents lists available at ScienceDirect

Biochemical and Biophysical Research Communications

journal homepage: www.elsevier.com/locate/ybbrc

Establishment of a humanized model of liver using NOD/Shi-*scid* IL2Rg^{null} mice

Hiroshi Suemizu [a,*,1], Masami Hasegawa [a,d,1], Kenji Kawai [b], Kenji Taniguchi [a,d], Makoto Monnai [a,e], Masatoshi Wakui [b,f], Makoto Suematsu [f], Mamoru Ito [c], Gary Peltz [g,2], Masato Nakamura [b,h]

[a] *Biomedical Research Department, Central Institute for Experimental Animals, 1430 Nogawa, Miyamae, Kawasaki, Kanagawa 216-0001, Japan*
[b] *Pathology Research Department, Central Institute for Experimental Animals, 1430 Nogawa, Miyamae, Kawasaki, Kanagawa 216-0001, Japan*
[c] *Laboratory Animals Research Department, Central Institute for Experimental Animals, 1430 Nogawa, Miyamae, Kawasaki, Kanagawa 216-0001, Japan*
[d] *Pharmaceutical Research Department II, Chugai Pharmaceutical Co., Ltd., 200 Kajiwara, Kamakura, Kanagawa 247-8530, Japan*
[e] *Chugai Research Institute for Medical Science, Inc., 200 Kajiwara, Kamakura, Kanagawa 247-8530, Japan*
[f] *Department of Biochemistry and Integrative Medical Biology, Keio University School of Medicine, 35 Shinanomachi, Shinjuku, Tokyo 160-8582, Japan*
[g] *Department of Genetics and Genomics, Roche Palo Alto, 3431 Hillview Avenue, Palo Alto, CA 94304-1397, USA*
[h] *Department of Pathology, Tokai University School of Medicine, 143 Shimokasuya, Isehara, Kanagawa 259-1193, Japan*

ARTICLE INFO

Article history:
Received 10 September 2008
Available online 7 October 2008

Keywords:
Humanized mouse
Liver repopulation
NOD/Shi-*scid* IL2Rg^{null} (NOG) mouse
Urokinase-type plasminogen activator

ABSTRACT

Severely immunodeficient NOD/Shi-*scid* IL2Rg^{null} (NOG) mice are used as recipients for human tissue transplantation, which produces chimeric mice with various types of human tissue. NOG mice expressing transgenic urokinase-type plasminogen activator in the liver (uPA-NOG) were produced. Human hepatocytes injected into uPA-NOG mice repopulated the recipient livers with human cells. The uPA-NOG model has several advantages over previously produced chimeric mouse models of human liver: (1) the severely immunodeficient NOG background enables higher xenogeneic cell engraftment; (2) the absence of neonatal lethality enables mating of homozygotes, which increased the efficacy of homozygote production; and (3) donor xenogeneic human hepatocytes could be readily transplanted into young uPA-NOG mice, which provide easier surgical manipulation and improved recipient survival.

The metabolism of xenobiotic compounds, including medicinal drugs, predominantly occurs in the liver. Due to the significant inter-species differences in many liver enzymes that mediate drug metabolism, the metabolism of candidate pharmaceuticals is usually initially evaluated *in vitro* using human cells or cell extracts [1,2] or *in vivo* in rodent models. Although *in vivo* pharmacokinetic studies are routinely performed in experimental animal models, significant inter-species differences in drug metabolism limit their ability to predict human drug metabolism. There are many examples where the findings from rodent models do not extrapolate to man. *In vitro* studies using transformed human hepatic cells, human hepatocytes or human hepatocyte extracts have also been used to predict human drug metabolism. Although they utilize human cells, *in vitro* systems have a very limited ability to predict human drug metabolism *in vivo*. Drug-induced alterations of the level of expression of drug metabolizing enzymes, which is a common problem in clinical medicine, does not occur in the *in vitro* extracts. In addition, the pattern of expression of drug metabolizing enzymes is altered within a very short time period after hepatocytes are cultured *in vitro* (reviewed in [2]). Human drug metabolizing enzymes have been expressed as transgenes in mice. For example, a mouse expressing a human CYP2D6 transgene in liver had a human-specific profile of metabolism of a test substrate [3]. However, transgenic expression of one or a few human enzymes in mouse liver does not represent the biotransformation capabilities of human liver.

To overcome the limitations associated with currently used *in vitro* and *in vivo* experimental methods for studying drug metabolism and toxicity, investigators have utilized several different methods for producing chimeric mice with artificial human livers. Historically, chimeric mice have been generated by introducing human tissues or cells into immune deficient SCID mice, which have an inactivating mutation in the catalytic subunit of the DNA-dependent protein kinase (Prkdc^{scid}, known as the *scid* mutation). Ralph Brinster and colleagues demonstrated that transgenic expression of urokinase-type plasminogen activator (AL-uPA) within mouse liver directed by an albumin promoter caused progressive damage to liver parenchymal cells [4,5]. The mice usually died within weeks due to progressive liver failure. Although the mechanism of hepatic cell destruction has not fully characterized in detail; uPA regulates the activation of plasminogen, which controls the activation of matrix metalloproteinases that are critical for liver cell growth (reviewed in [6]). In addition, the livers in surviving mice are replaced at 8–12 weeks of age by nodular growths that have deleted the transgene. In an elegant series of experi-

* Corresponding author. Fax: +81 44 754 4465/4454.
E-mail address: suemizu@ciea.or.jp (H. Suemizu).
[1] These authors contributed equally to this work.
[2] Present address: Department of Anesthesia, Stanford University, Stanford, CA 94305-5796, USA.

0006-291X/$ - see front matter © 2008 Elsevier Inc. All rights reserved.
doi:10.1016/j.bbrc.2008.09.124

ments, investigators showed that the AL-uPA mice could be rescued from liver failure by transplant of congenic or xenogenic hepatocytes [7–10]. Other investigators subsequently demonstrated that immunocompromised (recombinant activation gene-2; RAG-2 deficient or SCID mutation) mice expressing this transgene could be partially repopulated (~15%) with human hepatocytes [9,10].

Recently, we developed NOD/Shi-*scid* IL2Rg^{null} (NOG) mice by crossing IL-2 receptor gamma chain-deficient (IL2Rg^{null}) mice [11] with NOD/Shi-*scid* mice [12]. NOG mice lack T and B lymphocytes and natural killer (NK) cells, and they have impaired dendritic cell function [13–15]. Because of their severe immunodeficient state, NOG mice have been used as an *in vivo* model to study human hematopoietic stem cell [13,14] and endometrial tissue [16,17] engraftment. Here, we used NOG mice to develop an uPA/NOG-transgenic model that allows the engraftment of human hepatocytes into a damaged liver. This model could provide a useful tool for characterization of hepatic drug metabolism *in vivo* within a humanized liver.

Materials and methods

Transgenic mice. The mouse albumin promoter-driven urokinase-type plasminogen activator (*Plau*, known as uPA) gene expression unit (GenBank Accession No. AB453180) was constructed as follows. The 2345-bp *Not*I–*Bam*HI fragment of the mouse albumin enhancer/promoter from plasmid p2335A-1 [18], the 304-bp *Hin*dIII–*Nhe*I fragment of the chimeric intron from pCI plasmid (Promega Corp., WI, USA), the 1367-bp *Nhe*I–*Sal*I fragment of the PCR-amplified mouse uPA cDNA (MuPA-Nhe1-F, 5′-GCTA GCGGCACTACCATGAAAGTC-3′; MuPA-Sal1-R, 5′-AATTAAGTCGACA ACAAGTGACCC-3′), and the 624-bp *Sma*I–*Eco*RI fragment of the PCR-amplified human growth hormone (*GH1*) 3′-flanking region (hGHF, 5′-GCTCTACTGCTTCAGGAAGGACAT-3′; hGHR, 5′-GAATTCA ACAGGCATCTACTGA-3′) were cloned into the pBlueScript II vector (Promega) with appropriate polylinkers (5′-GATCCAAGCTTATGC AGTCGACCCGGGCATGCGAATTCTCGA-3′). A vector-free, 4.6-kb uPA expression fragment was prepared by *Not*I and *Kpn*I digestion and microinjected into fertilized NOD/Shi strain mouse eggs using standard methods. Transgenic founders were mated with NOD-Cg-*Prkdc*^{scid} *Il2rg*^{tm1Sug}/ShiJic (NOG) mice to confer the *scid* and IL2Rg^{null} mutations. The *scid* and IL2Rg^{null} mutations were genotyped by PCR as described previously [13,19]. The mice were assigned the following genetic designation: NOG-*Tg (Alb-Plau)11-4*/ShiJic [formally, NOD·Cg-*Prkdc*^{scid} *Il2rg*^{tm1Sug} *Tg(Alb-Plau)11-4*/ShiJic; abridged name: uPA-NOG]. The present study was performed in accordance with institutional guidelines and was approved by the Animal Experimentation Committee of the Central Institute for Experimental Animals.

Detection of uPA transcripts by RT-PCR. Total cellular RNA samples from the liver, kidney, and spleen were obtained from 29-week-old uPA-NOG mice using the RNeasy Mini kit (QIAGEN, Tokyo, Japan). Reverse transcription-polymerase chain reaction (RT-PCR) was performed using the High Capacity cDNA Reverse Transcription kit (Applera Corporation, CA, USA). The spMuPAF forward primer (5′-GAGGCACTGGGCAGGTGTCC-3′) and MuPAR reverse primer (5′-AGGGCCGACCTTTGGTATCAGTG-3′) were used to detect the spliced form of the external mouse uPA transcript (365-bp band). The 479-bp glyceraldehyde-3-phosphate dehydrogenase (*Gapdh*) fragment was amplified using the G3PDHF forward primer (5′-TCACCATCTTCCAGGAGCGAGA-3′) and the G3PDHR reverse primer (5′-GAAGGCCATGCCAGTGAGCTT-3′) and used as an internal control.

Spontaneous liver damage. The degree of liver damage was examined by determining the serum levels of alanine aminotransferase (ALT). Clinical biochemical analyses of serum samples were carried out with the Fuji DRI-CHEM 7000 (FUJIFILM Corporation, Tokyo, Japan).

Southern blot analyses. Genomic DNA samples from liver and kidney were obtained from 8-week-old uPA-NOG mice and non-transgenic mice by overnight incubation with proteinase K and subsequent extraction with phenol: chloroform: ethanol according to the standard protocol. *Xba*I, *Xho*I, *Bgl*II, and *Bam*HI restriction enzyme-digested genomic DNA was electrophoresed on a 0.6% agarose gel and transferred to a positively charged nylon membrane (F. Hoffmann-La Roche Ltd., Basel, Switzerland). Hybridization was carried out with a DIG-labeled probe that was prepared using the PCR DIG Probe Synthesis Kit (F. Hoffmann-La Roche Ltd.) using forward (5′-GTTCTCCAGCTTGGGATCGACCTG-3′) and reverse (5′-TTGATAGGAAAGGTGATCTGTGTGCAG-3′) primers according to the manufacturer's instructions.

Transplantation of human hepatocytes. Commercially available cryopreserved hepatocytes (Lonza Walkersville Inc., MD, USA) were used as donor cells. Young (6-week-old) uPA-NOG hemizygotes and homozygotes were used as recipients. Cell number and viability were determined by trypan blue exclusion in a hemocytometer. One million viable hepatocytes in 40 μl of Hank's Balanced Salt Solution (HBSS) were injected intrasplenically via a Hamilton syringe with a 26 G needle.

Human albumin measurements. Small volumes of blood were collected biweekly from the retro-orbital venousplexus with a plastic capillary. After a 500- to 30,000-fold dilution with Tris-buffered saline that contained 1% bovine serum albumin and 0.05% Tween-20, human albumin concentrations were measured with the Human Albumin ELISA Quantitation Kit (Bethyl Laboratories Inc., TX, USA) according to the manufacturer's protocol.

Immunoblotting. Diluted serum samples (2000× dilution) were solubilized in SDS sample buffer with 5% β-mercapthoethanol. Proteins were subjected to SDS–PAGE and transferred to Hybond-ECL membranes (GE Healthcare Bio-Sciences Corp., NJ, USA). The membranes were incubated for 90 min with biotinylated polyclonal goat anti-mouse albumin antibodies (A90-234A; Bethyl Laboratories) and biotinylated polyclonal goat anti-human albumin antibodies (A80-229A; Bethyl Laboratories), washed, and incubated with a streptavidin–horseradish peroxidase conjugate (GE Healthcare Bio-Sciences) for 60 min. The biotinylated antibodies were prepared using the FluoReporter Mini-Biotin-XX Protein Labeling Kit (Invitrogen Corp., CA, USA). The immunoblots were developed using the ECL Western Detection System and Hyperfilm ECL (GE Healthcare Bio-Sciences).

Histology and immunohistochemistry. The tissues were fixed with 4% (v/v) phosphate-buffered formalin, and paraffin-embedded sections were stained with hematoxylin and eosin (H&E). Polyclonal goat anti-human albumin antibodies (Bethyl Laboratories) were used as the primary antibodies. The antibodies were visualized using amino acid polymer/peroxidase complex-labeled anti-goat Ig antibody (Histofine Simple Stain Mouse MAX PO (G); Nichirei Bioscience Inc., Tokyo, Japan) and diamino-benzidine (DAB; Dojindo Laboratories, Kumamoto, Japan) substrate [0.2 mg/ml 3,3′-diaminobenzidinetetrahydrochloride, 0.05 M Tris–HCl (pH 7.6), and 0.005% H_2O_2]. Sections were counter-stained with hematoxylin.

Statistical analyses. Statistical analyses were performed with StatView ver. 5.0 (SAS Institute, Tokyo, Japan) and the Prism 5 software (GraphPad Software, CA, USA).

Results and discussion

Previously prepared AL-uPA transgenic mice [*Tg(Alb-1,Plau)Bri144* lines 1353–8 and lines 1944–6] possess five or 10 copies,

respectively, of the transgene joined head-to-tail in a tandem array [20]. In both lineages, half of the transgenic offspring bled extensively and died as neonates. Neonatal lethality was correlated with the level of expression of the uPA transgene, which is determined, at least in part, by the copy number. Therefore, we predicted that mice with fewer copies of the uPA transgene would have less liver damage, which would eliminate the uPA-mediated neonatal lethality. We produced uPA-transgenic mice in severely immunodeficient NOG mice [NOG-*Tg(Alb-Plau)11-4*/Shijic, referred to as uPA-NOG] with the uPA gene expression unit (Fig. 1A). RT-PCR analysis

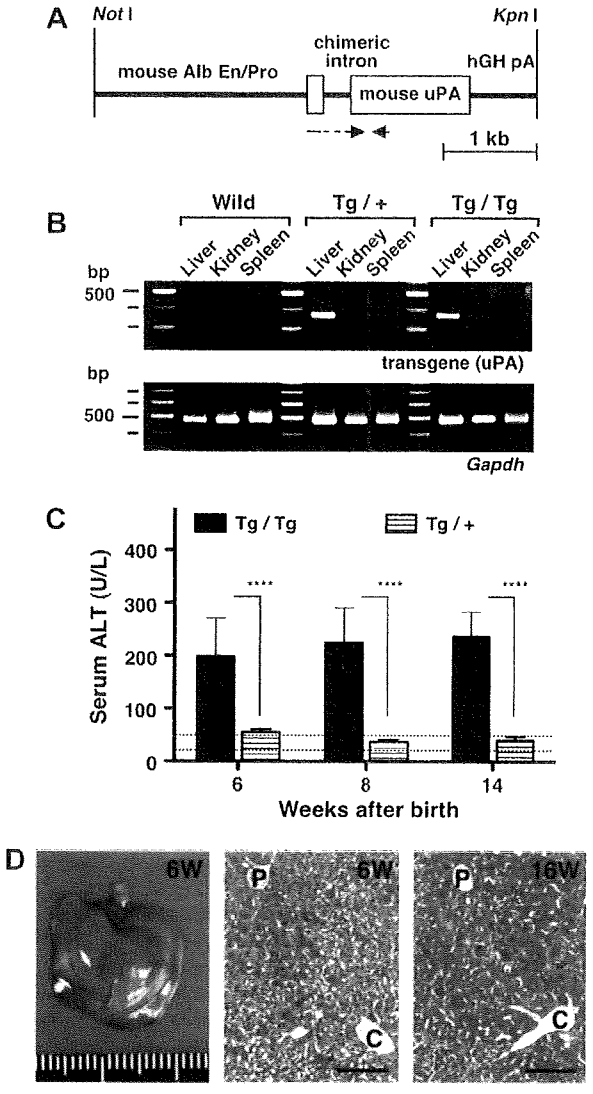

Fig. 1. Establishment of the uPA-NOG mouse as a model of spontaneous hepatic injury. (A) The uPA expression unit contains the mouse albumin enhancer/promoter (Alb En/Pro), the chimeric intron, mouse uPA cDNA, and the 3′-UTR of the human growth hormone gene with polyadenylation (pA) signal. Arrowheads depict the positions and directions of the RT-PCR primers. (B) RT-PCR analyses of uPA transgene expression. Wild, non-transgenic NOG; Tg/+, hemizygous; and Tg/Tg, homozygous uPA-NOG mice. *Gapdh* was used as an internal control. (C) ALT activities in uPA-NOG mice. All the values for the homozygous uPA-NOG (Tg/Tg) are significantly higher than those for the hemizygote (Tg/+) ($P < 0.0001$, unpaired *t*-test). Dashed lines indicate the two standard deviation ranges for the values for the non-transgenic NOG mice ($n = 7$). Each of the points for the hemizygous and homozygous uPA-NOG mice represent the mean ± SD of four to seven samples. (D) Gross appearance and histopathology of a homozygous uPA-NOG mouse liver. Scale bar, 100 μm; P, portal tract; C, central vein.

of uPA transgene expression indicated that the chimeric introns were appropriately spliced to produce the uPA expression unit. Although the transgene was expressed in the livers of hemizygous (Tg/+) and homozygous (Tg/Tg) uPA-NOG mice; it was not expressed in the kidneys, spleens or any other tissues obtained from non-transgenic NOG mice (Fig. 1B). uPA-NOG hemizygotes were indistinguishable from non-transgenic littermates; they have never exhibited spontaneous intestinal or intra-abdominal bleeding that was typically seen in previously produced AL-uPA transgenic mice [21]. The level of expression of the transgene in hemizygous uPA-NOG mice was below that required to cause liver disease. The serum ALT activity in the hemizygote, an indicator of hepatocyte damage, did not increase in mice at any age and was identical to that of a non-transgenic NOG mouse (Fig. 1C).

Since transgene zygosity affects the phenotype of transgenic mice via a gene dosage effect; we produced a homozygous line of uPA-NOG mice that carries two copies of the transgene array that stably reinforces transgene expression. To do this, female and male homozygotes were bred to produce homozygous uPA-NOG mice, which no longer needed progeny testing or genotyping for zygosity. At birth, the homozygotes, whose zygosity was confirmed by progeny testing, were slightly smaller than their hemizygous littermates. Quantitative RT-PCR revealed that transgene expression in the livers of homozygous uPA-NOG mice was 2.4- to 3.6-fold higher than hemizygotes (data not shown). However, perinatal hemorrhaging, embryonic lethality or neonatal lethality did not occur in homozygous uPA-NOG mice. The serum ALT level (75.0 ± 9.1, $n = 4$) in the homozygote at 4 weeks of age was slightly above that of the hemizygote, but this trend did not reach statistical significance (data not shown). However, the ALT levels began to increase by 6 weeks of age in the uPA-NOG homozygotes, and remained elevated through 14 weeks of age (Fig. 1C). The livers of 6-week-old uPA-NOG homozygotes had evidence of modest hepatic injury. The hepatocytes focally showed degeneration foci and a few eosinophilic bodies predominantly around the central veins (Fig. 1D, center). The livers of 16-week-old uPA-homozygous mice revealed megalocytosis with increased eosinophilic bodies (Fig. 1D, right).

The phenotype and liver histology of uPA-NOG mice was significantly different from that of previously produced AL-uPA transgenic mice. uPA-NOG mice did not develop the severe edema that was observed AL-uPA homozygote mice at 3–6 weeks of age [4]. The color of the liver parenchyma was also significantly different. The livers of 3- to 5-week-old AL-uPA-transgenic homozygotes were smooth and pale to nearly white in color (known as "white liver"), and the livers of the hemizygotes were also profoundly abnormal in appearance, with multiple reddish nodules in addition to the white parenchyma [4]. However, the liver of 6-week-old homozygous uPA-NOG mouse did not show any "white liver" changes, regardless of uPA transgene zygosity (Fig. 1D, left). AL-uPA transgenic mice have an age-dependent decrease in uPA expression that is caused by deletion of the integrated transgene [4]. However, Southern blot analysis indicated that the transgene array was stably integrated at a single locus in the uPA-NOG homozygote (Fig 2A). The fact that there were no differences in hybridization banding patterns in the liver and kidney DNA samples in 8-week-old uPA-NOG mice indicate that there is a relatively low frequency of physical loss of the transgene from uPA-NOG mice. Furthermore, stable level of expression of the uPA transgene (Fig. 1B) and the persistence of high levels of the hepatic injury marker (ALT) also indicate the transgene is stably expressed (data not shown). Further analysis of the banding pattern after *Xho*I digestion indicate that uPA-NOG mice have at least three copies of the 4.6-kb monomeric transgene. The low copy number of the integrated transgene in uPA-NOG mice may prevent neonatal lethality. The architecture of the integrated transgene in uPA-NOG mice was further analyzed by southern blot analyses with additional restric-

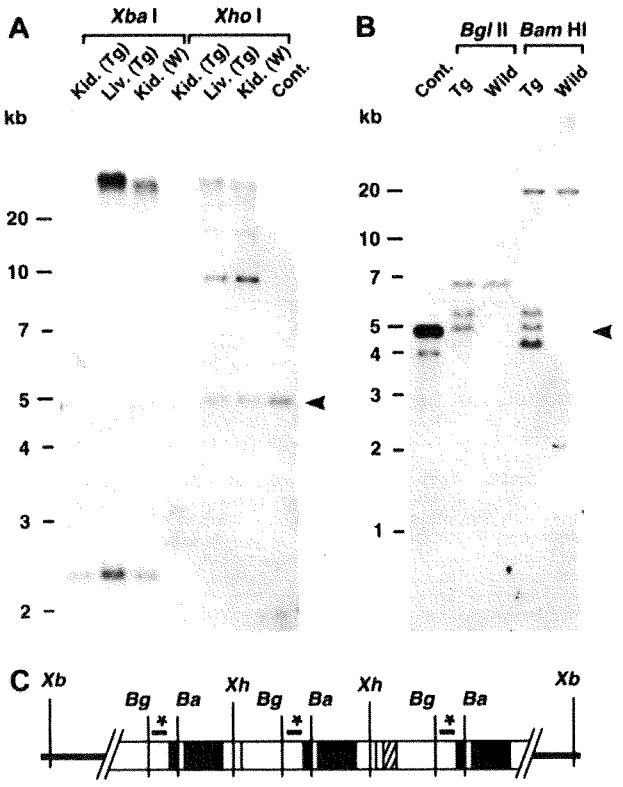

Fig. 2. Molecular analyses of the integrated transgene in uPA-NOG mice. (A) DNA samples from non-transgenic NOG mouse kidney (Kid.; W) and uPA-NOG hemizygote kidney (Kid.; Tg) and liver (Liv.; Tg) were digested with XbaI and XhoI for Southern blot analysis. (B) DNA samples from non-transgenic NOG mouse kidney (Wild) and uPA-NOG hemizygote kidney (Tg) was digested with BglII and BamHI. The uPA expression unit (4.6-kb fragment) was used as a positive control (arrowhead). (C) Restriction map and structure of the transgene in uPA-NOG mice. Solid boxes indicate transcribed segments. Asterisks indicate the positions recognized by DIG-labeled probes. The shaded box indicates the rearranged region. Restriction enzymes: Xb, XbaI; Xh, XhoI; Bg, BglII; Ba, BamHI.

tion enzymes (Fig 2B) to produce the restriction map of the integrated transgene array (Fig. 2C). This array consists of at least three copies of the uPA gene expression unit joined head-to-tail in a tandem array. One of the uPA gene expression units that located at downstream position had a small rearrangement (Fig. 2C). However, the rearrangement was likely not an acquired characteristic, because the rearrangement was observed in the founder mice from this line (data not shown).

To determine whether uPA-NOG mice could support repopulation by transplanted hepatocytes, commercially available cryopreserved human hepatocytes were transplanted into 6-week-old uPA-NOG hemizygous and homozygous recipients. The hepatocytes were successfully transplanted only into the homozygous uPA-NOG mice. Engraftment was demonstrated by different methods, including histology, human serum albumin measurements (ELISA), immunoblotting, and immunohistochemical staining (Fig. 3). At the time of transplantation, the recipient mice were clinically healthy and indistinguishable from non-transgenic uPA-NOG mice. Growth of transplanted human hepatocytes was not detectable in either the hemizygous or homozygous uPA-NOG mouse livers by gross inspection (Fig. 3A) because of the lack of obvious differences, such as color [8]. Periodic measurements of human albumin levels in the blood of each recipient were performed, to estimate repopulation of the mouse livers with human hepatocytes. Hemizygous recipients transplanted with human

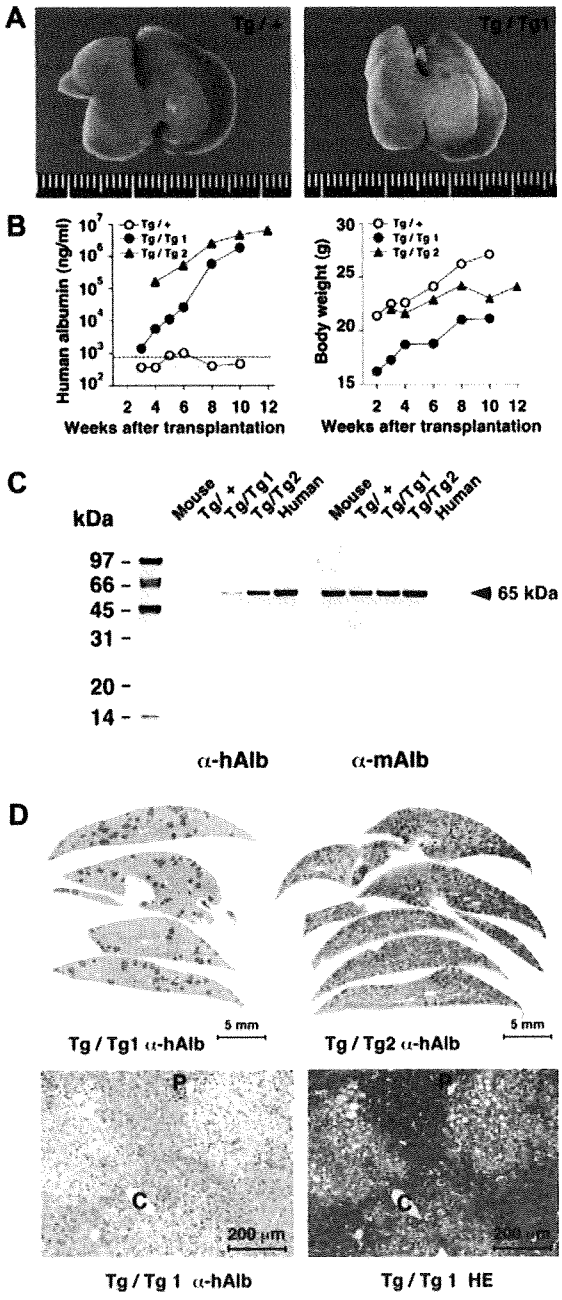

Fig. 3. Engraftment and repopulation of human hepatocytes in uPA-NOG mice. (A) Gross appearance of the uPA-NOG mouse liver 10 weeks after human hepatocyte transplantation. Tg/+, hemizygous; Tg/Tg, uPA-NOG homozygote. (B) Blood albumin concentrations in human cell recipients were assayed by ELISA. Dashed lines indicate the two standard deviation ranges for the values for the untransplanted uPA-NOG mice ($n = 6$). Body-weight changes after human hepatocyte transplantation are shown. (C) Immunoblot analysis shows human albumin (α-hAlb) and mouse albumin (α-mAlb) production in hemizygous (Tg/+) or homozygous (Tg/Tg) uPA-NOG transplant recipient mice. (D) Histology and immunohistochemistry of livers from uPA-NOG mice that were repopulated with human hepatocytes. Immunohistochemical staining for human albumin (top and lower left) and H&E staining (lower right). P, portal tract; C, central vein.

hepatocytes did not produce levels of human serum albumin that were indicative of a successful transplant (Fig. 3B, left); human albumin was not detected by immunoblotting (Fig. 3C, left) or

immunohistochemical staining (data not shown). Conversely, both homozygous recipients repopulated after transplantation of the human hepatocytes. These mice produced more than 1 mg/ml human albumin, and immunohistochemical staining suggested that the livers were comprised of at least 10–15% human hepatocytes (Fig. 3B, left). In one mouse, the circulating human serum albumin level continued to increase to 6.5 mg/ml. Although uPA-NOG hemizygotes and homozygotes both gained weight after transplantation (Fig. 3B, right), immunoblot analyses showed successful engraftment of the transplanted human hepatocytes in only the uPA-NOG homozygotes (Fig. 3C). Furthermore, human albumin was detected in the sera from both homozygotes (Tg/Tg1 and Tg/Tg2) with the anti-human albumin antibody; immunohistochemical staining for albumin further confirmed the human origin of these hepatocytes. Sera obtained from hemizygous uPA-NOG mice transplanted with human hepatocytes did not contain detectable amounts of human albumin. However, mouse albumin was detected in the sera from all of the mice.

Numerous mature human hepatocytes were identified in the livers of the transplanted uPA-NOG homozygotes (Fig. 3D, top). The number of human hepatocyte foci and the repopulation index, which was calculated based on the human hepatocyte/total liver cell number, appears to correspond to the measured blood levels of human albumin. In the Tg/Tg1 uPA-NOG homozygote, the blood human albumin levels reached 1.8 mg/ml, and the repopulation index was estimated to be 20% (Fig. 3D, upper and lower left). As mentioned previously, the human albumin levels reached 6.5 mg/ml in one mouse, a Tg/Tg2 uPA-NOG homozygote. In this mouse, almost 80% of the hepatocytes showed positive staining for human albumin, which suggests that the recipient liver was replaced by the transplanted human hepatocytes (Fig. 3D, top right). The human hepatocytes were fairly swollen and had a rarefied cytoplasm, such that these cells were easily discriminated from their murine counterparts (Fig. 3D, lower right). Periodic acid-Schiff (PAS) reaction showed that the empty spaces in these cells corresponded to areas of glycogen storage [22,23]. Furthermore, wisps and small clumps were evident in the cytoplasm, indicating that the organelles were displaced by excessive glycogen accumulation.

We anticipate that these humanized uPA-NOG mice will be useful for studying drug metabolism, general metabolic effects after hepatic engraftment, and the differentiation of stem cells for hepatocytes.

Acknowledgments

We thank Dr. R.D. Palmiter for providing plasmid p2335A-1, which carries the mouse albumin enhancer/promoter gene, S. Inoue, Y. Ando, M. Kuronuma, T. Mizushima, T. Kamisako, T. Etoh, and T. Ogura for their excellent technical assistance with animal experiments, C. Yagihashi and N. Omi for technical assistance with the molecular analyses, and Y. Ohnishi for helpful discussions. This work was supported by Grant-in-Aid for Scientific Research (17300136) as well as by Global COE Program for In vivo Human Metabolomic Systems Biology from MEXT.

References

[1] E.F. Brandon, C.D. Raap, I. Meijerman, J.H. Beijnen, J.H. Schellens, An update on in vitro test methods in human hepatic drug biotransformation research: pros and cons, Toxicol. Appl. Pharmacol. 189 (2003) 233–246.
[2] M.J. Gómez-Lechón, M.T. Donato, J.V. Castell, R. Jover, Human hepatocytes as a tool for studying toxicity and drug metabolism, Curr. Drug Metab. 4 (2003) 292–312.
[3] A.M. Yu, J.R. Idle, F.J. Gonzalez, Polymorphic cytochrome P450 2D6: humanized mouse model and endogenous substrates, Drug Metab. Rev. 36 (2004) 243–277.
[4] E.P. Sandgren, R.D. Palmiter, J.L. Heckel, C.C. Daugherty, R.L. Brinster, J.L. Degen, Complete hepatic regeneration after somatic deletion of an albumin-plasminogen activator transgene, Cell 66 (1991) 245–256.
[5] K.M. Braun, E.P. Sandgren, Liver disease and compensatory growth: unexpected lessons from genetically altered mice, Int. J. Dev. Biol. 42 (1998) 935–942.
[6] F.F. Mohammed, R. Khokha, Thinking outside the cell: proteases regulate hepatocyte division, Trends Cell Biol. 15 (2005) 555–563.
[7] J.A. Rhim, E.P. Sandgren, J.L. Degen, R.D. Palmiter, R.L. Brinster, Replacement of diseased mouse liver by hepatic cell transplantation, Science 263 (1994) 1149–1152.
[8] J.A. Rhim, E.P. Sandgren, R.D. Palmiter, R.L. Brinster, Complete reconstitution of mouse liver with xenogeneic hepatocytes, Proc. Natl. Acad. Sci. USA 92 (1995) 4942–4946.
[9] D.F. Mercer, D.E. Schiller, J.F. Elliott, D.N. Douglas, C. Hao, A. Rinfret, W.R. Addison, K.P. Fischer, T.A. Churchill, J.R. Lakey, D.L. Tyrrell, N.M. Kneteman, Hepatitis C virus replication in mice with chimeric human livers, Nat. Med. 7 (2001) 927–933.
[10] M. Dandri, M.R. Burda, E. Török, J.M. Pollok, A. Iwanska, G. Sommer, X. Rogiers, C.E. Rogler, S. Gupta, H. Will, H. Greten, J. Petersen, Repopulation of mouse liver with human hepatocytes and in vivo infection with hepatitis B virus, Hepatology 33 (2001) 981–988.
[11] K. Ohbo, T. Suda, M. Hashiyama, A. Mantani, M. Ikebe, K. Miyakawa, M. Moriyama, M. Nakamura, M. Katsuki, K. Takahashi, K. Yamamura, K. Sugamura, Modulation of hematopoiesis in mice with a truncated mutant of the interleukin-2 receptor gamma chain, Blood 87 (1996) 956–967.
[12] Y. Koyanagi, Y. Tanaka, J. Kira, M. Ito, K. Hioki, N. Misawa, Y. Kawano, K. Yamasaki, R. Tanaka, Y. Suzuki, Y. Ueyama, E. Terada, T. Tanaka, M. Miyasaka, T. Kobayashi, Y. Kumazawa, N. Yamamoto, Primary human immunodeficiency virus type 1 viremia and central nervous system invasion in a novel hu-PBL-immunodeficient mouse strain, J. Virol. 71 (1997) 2417–2424.
[13] M. Ito, H. Hiramatsu, K. Kobayashi, K. Suzue, M. Kawahata, K. Hioki, Y. Ueyama, Y. Koyanagi, K. Sugamura, K. Tsuji, T. Heike, T. Nakahata, NOD/SCID/gamma(c)(null) mouse: an excellent recipient mouse model for engraftment of human cells, Blood 100 (2002) 3175–3182.
[14] T. Yahata, K. Ando, Y. Nakamura, Y. Ueyama, K. Shimamura, N. Tamaoki, S. Kato, T. Hotta, Functional human T lymphocyte development from cord blood $CD34^+$ cells in nonobese diabetic/Shi-scid, IL-2 receptor gamma null mice, J. Immunol. 169 (2002) 204–209.
[15] M. Ito, K. Kobayashi, T. Nakahata, NOD/Shi-scid IL2rgamma(null) (NOG) mice more appropriate for humanized mouse models, Curr. Top. Microbiol. Immunol. 324 (2008) 53–76.
[16] H. Masuda, T. Maruyama, E. Hiratsu, J. Yamane, A. Iwanami, T. Nagashima, M. Ono, H. Miyoshi, H.J. Okano, M. Ito, N. Tamaoki, T. Nomura, H. Okano, Y. Matsuzaki, Y. Yoshimura, Noninvasive and real-time assessment of reconstructed functional human endometrium in NOD/SCID/gamma c(null) immunodeficient mice, Proc. Natl. Acad. Sci. USA 104 (2007) 1925–1930.
[17] R. Matsuura-Sawada, T. Murakami, Y. Ozawa, H. Nabeshima, J. Akahira, Y. Sato, Y. Koyanagi, M. Ito, Y. Terada, K. Okamura, Reproduction of menstrual changes in transplanted human endometrial tissue in immunodeficient mice, Hum. Reprod. 20 (2005) 1477–1484.
[18] C.A. Pinkert, D.M. Ornitz, R.L. Brinster, R.D. Palmiter, An albumin enhancer located 10 kb upstream functions along with its promoter to direct efficient, liver-specific expression in transgenic mice, Genes Dev. 1 (1987) 268–276.
[19] C. Maruyama, H. Suemizu, S. Tamamushi, S. Kimoto, N. Tamaoki, Y. Ohnishi, Genotyping the mouse severe combined immunodeficiency mutation using the polymerase chain reaction with confronting two-pair primers (PCR-CTPP), Exp. Anim. 51 (2002) 391–393.
[20] E.P. Sandgren, R.D. Palmiter, J.L. Heckel, R.L. Brinster, J.L. Degen, DNA rearrangement causes hepatocarcinogenesis in albumin-plasminogen activator transgenic mice, Proc. Natl. Acad. Sci. USA 89 (1992) 11523–11527.
[21] J.L. Heckel, E.P. Sandgren, J.L. Degen, R.D. Palmiter, R.L. Brinster, Neonatal bleeding in transgenic mice expressing urokinase-type plasminogen activator, Cell 62 (1990) 447–456.
[22] P. Meuleman, L. Libbrecht, R. De Vos, B. de Hemptinne, K. Gevaert, J. Vandekerckhove, T. Roskams, G. Leroux-Roels, Morphological and biochemical characterization of a human liver in a uPA-SCID mouse chimera, Hepatology 41 (2005) 847–856.
[23] H. Azuma, N. Paulk, A. Ranade, C. Dorrell, M. Al-Dhalimy, E. Ellis, S. Strom, M.A. Kay, M. Finegold, M. Grompe, Robust expansion of human hepatocytes in Fah−/−/Rag2−/−/Il2rg−/−mice, Nat. Biotechnol. 25 (2007) 903–910.

Available online at www.sciencedirect.com
ScienceDirect
Comparative Immunology, Microbiology & Infectious Diseases 31 (2008) 347–366
COMPARATIVE IMMUNOLOGY MICROBIOLOGY & INFECTIOUS DISEASES
www.elsevier.com/locate/cimid

Histopathological classification of systemic *Mycobacterium avium* complex infections in slaughtered domestic pigs

Kenji Hibiya[a,*], Yuko Kasumi[b], Isamu Sugawara[b], Jiro Fujita[a]

[a] *Department of Medicine and Therapeutics, Control and Prevention of Infectious Diseases, Faculty of Medicine, University of the Ryukyus, 207 Uehara, Nishihara, Okinawa 903 0215, Japan*
[b] *Mycobacterium Reference Centre, Research Institute of Tuberculosis, 3-1-24 Matsuyama, Kiyose-shi, Tokyo 204 0022, Japan*

Accepted 16 May 2007

Abstract

The aim of this study was to classify the histopathological features of pigs infected with *Mycobacterium avium* complex (MAC). We used slaughtered pig organs systemically infected with MAC. The results showed granulomatous lesions which were observed predominantly in the digestive organs and regional lymph nodes rather than respiratory organs. The histological picture showed a wide range of granulomatous stages from exudative to fibrotic reactions to the MAC infection. Eosinophils and giant cells were characteristically observed in the exudative reactions. The histopathological type in primary focus tended to be maintained in the respective organs. Most strains with the same genotype showed pathogenicity for guinea pigs irrespective of the type of granuloma. Although these findings suggest that different stages of a granulomatous lesion originating from the same causative agent might influence histological patterns, other possibilities such as the hereditary background of the host, or the effects of viral infections should be considered.

Keywords: *Mycobacterium avium* complex; Classification; Histopathological; Granuloma; IS*1245*; Pigs

*Corresponding author. Tel.: +81 98 895 1144; fax: +81 98 895 1414.
E-mail address: k068736@eve.u-ryukyu.ac.jp (K. Hibiya).

0147-9571/$ - see front matter © 2007 Elsevier Ltd. All rights reserved.
doi:10.1016/j.cimid.2007.05.001

Résumé

L'objectif de cette étude est de classifier les caractéristiques histopathologiques des porcs infectés par le complexe *Mycobacterium avium* (MAC). Nous avons examiné des organes de porcs abattus, infectés par le MAC. Les résultats ont montré des lésions granulomateuses observées principalement dans les organes digestifs et les ganglions lymphatiques environnants plus que dans les organes respiratoires. Les schémas histopathologiques ont montré une grande diversité de stades granulomateux, allant de réactions exudatives jusqu'à des réactions fibrotiques. Les eosinophiles et les cellules géantes ont été particulièrement observées dans les réactions exudatives. La plupart des souches de bactéries présentant le même génotype ont montré un pouvoir pathogène chez les cobayes, indépendamment du type granulomateux. Bien que ces résultats suggèrent que différents stades d'une lésion granulomateuse ayant pour origine la même bactérie puissent révéler leurs influences sur les schémas histopathologiques, d'autres possibilités telles que l'hérédité du sujet ou les effets d'une potentielle infection virale doivent également être prises en compte.

Mots clés: Le Complexe *Mycobaterium avium* (MAC); Classification; Histopathologie; Granulome; Séquence d'insertion génomique (IS) *1245*; Porcs

1. Introduction

Mycobacterium avium complex (MAC) infection occurs in immunocompromised hosts or patients with antecedent pulmonary diseases [1]. Recently, the study of pulmonary MAC diseases in patients without a predisposing condition has become very significant for this common clinical problem [2,3]. Such types of MAC diseases cause extensive granuloma formation in the airway and have a progressive course [4]. Therefore, the study of MAC infections is a critical issue.

Some previous studies have reported pathological findings of typical mycobacteriosis, such as leprosy and tuberculosis [5,6]. Ridley subdivided the histopathological picture of leprosy into two main spectrums: (1) tuberculoid granulomas; and (2) lepromatous granulomas [5]. However, controversy exist as to whether or not these classical notions can be applied generally to granulomatous responses to MAC infection in humans. Two spectrums of epithelioid cell granuloma with or without caseation necrosis were observed in human MAC infections [7]. Undifferentiated granuloma was observed in the septic focus with MAC in acquired immunodeficiency syndrome (AIDS) [8–12]. However, whether such histological responses have been maintained among the organs in systemically infected individuals has not been well understood in previous investigations. Since it is very difficult to obtain affected tissues in humans, the evaluation of histopathological findings in MAC patients has not been well defined [4,13].

The domestic pig is an animal susceptible to MAC. In fact, sporadic epidemic outbreaks have occurred throughout the world [14–18]. This has allowed us to engage in relatively extensive histological analyses of the same disease stages due to a large number of pigs being slaughtered during the same growth period in nations

where a modern pig industry is well established [19]. There is the possibility of the pig MAC infection serving an alternative model for MAC infection in human beings.

Some histopathological evaluations of pigs infected with MAC have previously been described [15,20–22]. Histopathological change from a proliferative to an infiltrative character has been observed in lesions of these pigs [20,22]. They demonstrated that dissemination of MAC occurs in domestic pigs. Ellsworth et al. reported that an aborted sow infected with MAC show focal non-encapsulated granulomas in lymph nodes, tonsils, kidney, liver, spleen, lungs as well as the uterine and vaginal walls [23]. However, specific details of the histopathological features have not been demonstrated [15,20]. Moreover, it is not clear whether strains with certain genotypes cause specific histopathological features or whether the features were formed by host reactions.

The aim of the present study was to evaluate the histopathological features of systemically infected domestic pigs. We, then, examined the relationships among the histopathological types, their pathogenesis, and the genotypes of strains.

2. Materials and methods

2.1. Materials for histological examination

We collected organs with granulomatous lesions from pigs ($n = 403,792$) slaughtered in Okinawa prefecture between 2002 and 2004. The granulomatous lesions were macroscopically assessed by trained veterinary meat inspectors. The assessment criteria were based on the provisions stipulated in the Standard Procedure Manual of the Japanese National Meat Hygiene Inspection Organization. Thus, the sub-maxillary and mesenteric lymph nodes as well as the liver of the pigs were routinely examined. The sub-maxillary lymph nodes and the mesenteric lymph nodes were incised. The lesions of the lymph nodes were characterized by caseous foci, ranging in size from a pinhead to a broad bean. We distinguished the granulomatous lesions from other similar conditions like nodules caused by toxoplasmosis and milk-spots due to ascarid infections in the liver. We inspected other organs and regional lymph nodes in more detail when we observed caseous lesions in the liver.

We decided to use systemically infected pigs ($n = 276$) as the objective material for this study. A systemically infected pig was defined as a carcass with granulomatous lesions found macroscopically in the sub-maxillary or mesenteric lymph nodes, and any of the visceral organs such as the liver, lung, or spleen, which were routinely examined. All oriented pigs were clinically silent. There was no significant difference in the mean weight between the systemically infected pigs with MAC and the other slaughtered pigs (mean carcass weight was 76.8 kg [$n = 218$ for systemically infected pigs] and 79.5 kg [$n = 21,569$ for the other pigs shipped during the fixed period]).

2.2. Histological examination

Tissue ($n = 3312$: 276 pigs $\times$ 12 tissues) from systemically infected pigs was used as material for the histopathological examination. The affected tissues was